A&A 424, 1003–1010 (2004)
DOI: 10.1051/0004-6361:20040497

Astronomy & Astrophysics

Properties of longitudinal flux tube waves

III. Wave propagation in solar and stellar wind flows

M. Cuntz[1] and S. T. Suess[2]

[1] Department of Physics, Science Hall, University of Texas at Arlington (UTA), Arlington, TX 76019-0059, USA
e-mail: cuntz@uta.edu
[2] NASA Marshall Space Flight Center, Space Science Laboratory, Mail Stop SD 50, Huntsville, AL 35812, USA
e-mail: steven.t.suess@nasa.gov

Received 22 March 2004 / Accepted 25 May 2004

Abstract. We discuss the analytic properties of longitudinal tube waves taking into account ambient wind flows. This is an extension of the studies of Papers I and II, which assumed a mean flow speed of zero and also dealt with a simplified horizontal pressure balance. Applications include the study of longitudinal flux tube waves in stars with significant mass loss and the heating and dynamics of plumes in the solar wind. Slow magnetosonic waves, also called longitudinal waves, have been observed in solar plumes and are likely an important source of heating. We show that the inclusion of ambient wind flows considerably alters the limiting shock strength as well as the energy damping length of the waves.

Key words. magnetohydrodynamics (MHD) – shock waves – Sun: solar wind – stars: winds, outflows

1. Introduction

The propagation of longitudinal flux tube waves has been extensively studied in the past and various detailed numerical simulations have been obtained for different types of stars including the Sun. The main focus of these models is the description of MHD flux tube heating above photospheric magnetic elements (e.g., Spruit 1981, 1982; Roberts 1983; Herbold et al. 1985; see also reviews by Narain & Ulmschneider 1990, 1996). It has been shown that MHD flux tube heating increases with increasing magnetic filling factor and that the amount of heating critically depends on the tube spreading, i.e. the change of the tube cross section with height (Rammacher & Ulmschneider 1989; Fawzy et al. 1998). The previous papers in this series (Cuntz 1999, 2004; hereafter Papers I and II, respectively) describe analytic properties of longitudinal flux tube waves, including the effects of spreading. Paper I gives the derivation of the shock amplitude relations. It is shown that the shock amplitude relations can successfully be decoupled in linear approximation. Paper II deals with properties of propagating shocks. In this paper, a general analytic formula for the *limiting shock strength* is derived for different atmospheric structures, tube spreadings and values of plasma-β. It is found that a height-independent limiting strength is attained only for constant cross section tubes and exponential tubes. In all other cases, the shock strength is found to decrease with height, a behavior already confirmed by time-dependent simulations (Fawzy et al. 1998; Cuntz et al. 1998, 1999).

In Paper II, two important simplifications were made. First, it was assumed that the mean flow carrying the waves is zero, i.e., no wind patterns exist. Second, it was assumed that the flux tubes are embedded in a non-magnetic medium which led to a simplified description of the horizontal pressure balance. Magnetic fields outside of individual flux tubes exist, however, within all magnetic surface elements (e.g., Schüssler et al. 1994; Schrijver & Title 2003) and are thus universally important. The simplification that there is no significant wind flow is acceptable for chromospheric flux-tubes of most types of stars, particularly coronal main-sequence stars owing to their small chromospheric extents and low mass-loss rates (e.g., Linsky 1980; Holzer & MacGregor 1985; Jordan & Linsky 1987; Wood et al. 2002). Exceptions may include, however, evolved stars with extended chromospheres and significant mass loss with MHD flux tube heating being present (e.g., Solanki 1996). Other important exceptions include flow patterns in coronal fine structure of solar-type stars including the Sun, such as solar plumes. Wood et al. (2002) provided mass loss rates for a set of solar-like GK dwarfs by interpreting Lyman-α absorption in the hydrogen walls around those stars thus replacing earlier untested upper limits.

Plumes are bright rays in coronal holes seen from 1 to at least 30 $R_\odot$, although they fade with respect to the background above 10 $R_\odot$. Plumes have been observed and studied for decades and numerous descriptions of their empirical properties exist (e.g., Koutchmy & Bocchialini 1998; Gabriel et al. 2003). The investigation of plumes is also part of the

SOHO mission. Time-independent properties of plumes were given by Del Zanna et al. (1997) by solving the steady, ideal, 2-D MHD equations assuming azimuthal symmetry around the plume axis. Their method allowed to reproduce basic features of coronal plumes such as the super-radial expansion close to the base. Detailed studies emphasizing the importance of tube spreading were given by Habbal et al. (1995), Hu et al. (1997), and Suess et al. (1998), and others. Plumes exhibit a range of interesting time-dependent phenomena such as slow magnetosonic waves, a synonym of longitudinal flux tube waves, and Alfvén waves (e.g., Casalbuoni et al. 1999, and references therein).

Observations which point to the existence of slow magnetosonic waves were first described by Ofman et al. (1997, 1998) who found indications of quasi-periodic variations in the polarized brightness in the polar coronal holes between 1.9 and 2.45 $R_\odot$ in observations of the Ultraviolet Coronal Spectrometer (UVCS). Similar observations with the EUV Imaging Telescope (EIT) were given by DeForest & Gurman (1998) and interpreted in terms of quasi-periodic waves with periods of 10−15 min. Ofman et al. (1999) studied the height-dependent behavior of the wave amplitudes. They presented a first nonlinear MHD simulation and found that the existence of slow magnetosonic waves in plumes is consistent with observations assuming typical coronal conditions. Cuntz & Suess (2001) investigated the height of shock formation in plumes. The models take into account plume geometric spreading, heat conduction and radiative damping. They show that shock formation occurs at rather low coronal heights, typically between 1.1 and 1.3 $R_\odot$, depending on the wave parameters. This implies that shock heating in solar coronal plumes is expected to be relevant at most heights. For further results see Ofman et al. (2000).

In order to further pursue the analytic study of longitudinal flux tube waves, we generalize the assumptions of Papers I and II. The following modifications are pursued. First, we assume that the shocks are superimposed on a nonzero mean flow. Second, we consider a generalized horizontal pressure balance assuming that the tubes are embedded in a magnetized environment. As shown below, these effects do not change the Rankine-Hugoniot relations and do not alter the shock amplitude relations. However, they affect the equations of shock propagation as they modify the limiting shock strength as well as the scale height of the energy dissipation. This will be discussed in Sect. 2. In Sect. 3, we present applications to solar plumes. Section 4 gives our conclusions.

2. Basic equations

2.1. Longitudinal flux tube waves with stellar wind

We consider a thin, vertically oriented magnetic flux tube embedded in an external medium. Contrary to Papers I and II, we do not assume the external medium to be non-magnetic. We take into account that the mean flow speed may not necessarily be identically zero, allowing for the presence of wind flows in the region heated by longitudinal waves. The magnetohydrodynamic equations in the thin flux tube approximation, consisting of the continuity, momentum, horizontal pressure balance, and energy equation, can be written as

$$\frac{\partial}{\partial t}\left(\frac{\rho}{B}\right)+\frac{\partial}{\partial r}\left(\frac{\rho u}{B}\right)=0, \tag{1}$$

$$\frac{\partial u}{\partial t}+u\frac{\partial u}{\partial r}+\frac{1}{\rho}\frac{\partial p}{\partial r}+g=0, \tag{2}$$

$$p+\frac{B^2}{8\pi}=p_\mathrm{e}+\frac{B_\mathrm{e}^2}{8\pi}, \tag{3}$$

$$\frac{\partial S}{\partial t}+u\frac{\partial S}{\partial r}=\left.\frac{\mathrm{d}S}{\mathrm{d}t}\right|_\mathrm{Rad}. \tag{4}$$

Here ρ is the density, p the gas pressure, S the entropy, u the gas velocity and B the magnetic field strength in the tube. They are functions of radius r and time t. p_e and B_e are the gas pressure and magnetic field strength, respectively, outside the tube and g is the gravity, which are functions of r only. In addition, we assume the validity of the ideal gas law. The Eqs. (1) to (4) are therefore sufficient for computing the five quantities ρ, p, S, u and B, because only two of the three thermodynamic variables are independent.

The Alfvén wave speed c_A and plasma-β are given by

$$c_\mathrm{A}=\frac{B}{\sqrt{4\pi\rho}} \tag{5}$$

and

$$\beta=\frac{2p}{\rho c_\mathrm{A}^2}, \tag{6}$$

respectively. Similar to Paper I, we introduce $\tilde{\epsilon}=p_\mathrm{e}{:}p$ as ratio between the external and internal gas pressure. Considering that the magnetic field outside of the tube is not necessarily zero leads to the identity

$$\tilde{\epsilon}=\left(1+\frac{1}{\beta}\right)\cdot\left(1+\frac{1}{\beta_\mathrm{e}}\right)^{-1} \tag{7}$$

with β and β_e as plasma-β inside and outside the tube, respectively.

2.2. Rankine–Hugoniot relations

Now let us discuss the shock properties of longitudinal flux tube waves. Shocks are formed when waves propagate through a medium of decreasing density as also found for acoustic waves. The Rankine–Hugoniot relations for longitudinal tube waves are given by

$$\rho_1 v_1 A_1=\rho_2 v_2 A_2, \tag{8}$$

$$A_1\left(\rho_1 v_1^2-\frac{B_1^2}{4\pi}\right)=A_2\left(\rho_2 v_2^2-\frac{B_2^2}{4\pi}\right), \tag{9}$$

$$\frac{1}{2}v_1^2+H_1=\frac{1}{2}v_2^2+H_2. \tag{10}$$

Here ρ_1 is the density, A_1 is the tube cross section, B_1 is the magnetic field strength, v_1 the gas velocity, p_1 the gas pressure

and H_1 the enthalpy in front of the shock. Values with index 2 refer to the state behind the shock. The velocities v_1 and v_2 are measured in the frame that moves with the shock.

Note that the Rankine-Hugoniot relations Eqs. (8) to (10) remain unchanged by the presence of wind flows, since v_1 and v_2 only depend on the *relative* velocity between the gas and the shock. Also, the modified horizontal pressure balance (see Eq. (3)) does not alter Eq. (9) relative to Eq. (12) of Paper I because the magnetic field strengths B_1 and B_2 *inside the tube* enter the equation in the same way. The enthalpy H_1 in front of the shock is given by

$$H_1 = \frac{\gamma}{\gamma - 1}\frac{p_1}{\rho_1} = \frac{c_{\rm S1}^2}{\gamma - 1} \tag{11}$$

with an equivalent expression holding for H_2 (see Eq. (16), Paper I). Here we assume an ideal gas with $\gamma = 5/3$. p_1 and $c_{\rm S1}$ denote the pressure and adiabatic sound speed in front of the shock, respectively.

The transformation of the gas velocity from the laboratory (Euler) frame into the shock frame is given by

$$v_1 = u_1 - U_{\rm sh}, \quad v_2 = u_2 - U_{\rm sh}, \tag{12}$$

where $U_{\rm sh}$ is the shock speed in the laboratory frame. Here the gas velocities u_1, u_2 follow from the identities

$$u_1 = u_{\rm o} - u_{\rm m}, \quad u_2 = u_{\rm o} + u_{\rm m}, \tag{13}$$

with $u_{\rm m}$ as velocity amplitude. Following the notation of Paper I, $u_{\rm o} = u_{\rm o}(r)$ is the mean flow velocity with the shocks being superimposed.

The shock strength (or Mach number) $M_{\rm s}$ is given by

$$M_{\rm s} = \frac{U_{\rm sh} - u_1}{c_{\rm T1}} = 1 + \hat{\alpha}, \tag{14}$$

where u_1 and $c_{\rm T1}$ is the flow speed and tube speed in front of the shock, respectively, and $\hat{\alpha}$ is the residual shock strength for weak shocks (see Paper I). For shocks of given strength, the shock speed $U_{\rm sh}$ is altered to $u_{\rm o} + U_{\rm sh}$ because of the mean flow velocity.

Similar to Paper I, we can also give the shock amplitude relations for shocks of small strength (see Appendix A), which are not affected by a (nonzero) mean flow speed. Note that all quantities in the shock amplitude relations only depend on $\hat{\alpha}$ and plasma-β and can easily be computed if these values are known.

2.3. Wave energy flux and wave action density

In Paper II (see Eq. (27)) we already derived the wave energy flux per unit area given by $F_{\rm M} = \mathcal{F}_{\rm M}/A$. Assuming that the shocks are superimposed on a wind of velocity $u_{\rm o}(r)$, the definition of the wave energy flux now reads

$$F_{\rm M} = \frac{1}{P}\int_0^P (p - p_{\rm o})(u - u_{\rm o}){\rm d}t. \tag{15}$$

As we again consider sawtooth shock waves, we have $p = p_{\rm o} - p_{\rm m} + 2p_{\rm m}t/P$ and $u = u_{\rm o} - u_{\rm m} + 2u_{\rm m}t/P$ with $p_{\rm o}(r)$, as atmospheric pressure and P as wave period. Here $p_{\rm m}$ and $u_{\rm m}$ denote the pressure and velocity amplitude, respectively (see Appendix A). The wave energy flux $F_{\rm M}$ is then given by

$$F_{\rm M} = \frac{1}{3}\, p_{\rm m} u_{\rm m}, \tag{16}$$

which can also be expressed by

$$F_{\rm M} = \frac{4\gamma(1 + \frac{1}{2}\beta\gamma)^3 p_{\rm o} c_{\rm To}}{3(1 + \frac{3}{2}\beta\gamma + \gamma)^2}\, \hat{\alpha}^2 \tag{17}$$

with $c_{\rm To}$ as tube speed of the undisturbed wind. The dissipation rate ϵ of the shocks is given by

$$\epsilon = \frac{16}{3}\, \frac{\gamma(\gamma + 1)(1 + \frac{1}{2}\beta\gamma)^3 p_{\rm o}}{(1 + \frac{3}{2}\beta\gamma + \gamma)^3 P}\, \hat{\alpha}^3 \tag{18}$$

(see Eq. (19), Paper II). It should be noted that the expressions for the wave energy flux and the energy dissipation rate are unaltered relative to the case of Paper II, as they only depend on the relative jumps of the flow speed and pressure as well as various quantities of the undisturbed atmosphere excluding $u_{\rm o}$, i.e. the velocity of the wind.

Analogous to the case of acoustic waves, however, the wind is highly relevant for the *propagation* of the waves and energy dissipation length inspite of the fact that the sound is being "carried along" by the moving medium (e.g., Landau & Lifshitz 1987). Appropriate expressions can be obtained in the particular case of a slowly varying medium, i.e. with the wavelengths shorter than the scalelength of the changes in the wind velocity (Bretherton 1970). Even in the absence of dissipation of the waves, their energy density $\mathcal{E}$ is not a conserved quantity of the flow because of the interaction of the wave with the accelerating (or de-accelerating) gas in the wind (e.g., Bretherton 1970; Jacques 1977; Pijpers & Hearn 1989). The wave action density, however, defined by

$$\mathcal{A}_{\rm w} = \frac{\mathcal{E}}{\omega - uk} \tag{19}$$

is conserved. Here $\omega = 2\pi/P$ is the circular wave frequency, u the velocity, and $k = 2\pi/\lambda$ the wave number with λ as wavelength. We also find

$$\frac{\partial \mathcal{A}_{\rm w}}{\partial t} = \nabla \cdot (V_{\rm w}\mathcal{A}_{\rm w}) \tag{20}$$

with $V_{\rm w}$ as wave group velocity, which in our case is given as $u_{\rm o} + c_{\rm To}$.

The integration of Eq. (20) together with Eq. (19) yields

$$\frac{V_{\rm w}\mathcal{E}A}{\omega - uk} = {\rm const.}, \tag{21}$$

which describes the conservation of wave action density for generalized geometry in the absence of dissipation (Jacques 1977). Here $A = A_{\rm o}(r)$ denotes the area function (see Paper II). Note that both sides of Eq. (21) can be multiplied by ω as we only consider monochromatic waves. In this case we find

$$\frac{\omega}{\omega - uk} = \frac{c_{\rm To} + u_{\rm o}}{c_{\rm To}} \tag{22}$$

with $u = u_{\rm o}$. Here $u_{\rm o}$ and $c_{\rm To}$ are the flow speed and tube speed, respectively, which are both functions of height.

With $\mathcal{E} = F_{\rm M}/c_{\rm To}$ we obtain as identity for the propagation of longitudinal waves in stellar winds

$$\frac{\rm d}{{\rm d}r}\left(A\ F_{\rm M}\ \frac{(c_{\rm To}+u_{\rm o})^2}{c_{\rm To}^2}\right) = 0. \tag{23}$$

Equation (23) can easily be generalized for the case of dissipation. In addition, the presence of a nonzero flow speed $u_{\rm oo} = u_{\rm o}(r_{\rm o})$ at the inner boundary of the flux tube (or plume) can also be considered. We then obtain

$$\frac{1}{A}\frac{\rm d}{{\rm d}r}\left(\frac{A\ F_{\rm M}\ (c_{\rm To}+u_{\rm o})^2}{(c_{\rm To}+u_{\rm oo})^2}\right) = -\epsilon. \tag{24}$$

The wave energy flux $F_{\rm M}$ is given by Eq. (17) and the energy dissipation rate ϵ by Eq. (18). A similar expression for acoustic waves in spherically-symmetric winds has been given by Pijpers & Hearn (1989).

Finally, we introduce the Mach number of the wind as

$$M_{\rm w} = \frac{u_{\rm o}}{c_{\rm To}}. \tag{25}$$

If further assumed that the flow speed at the inner boundary of the tube (or plume) is small compared to the tube speed, i.e. $u_{\rm oo} \ll c_{\rm To}$, as found in most applications, we obtain

$$\frac{1}{A}\frac{\rm d}{{\rm d}r}\left(A\ F_{\rm M}\ (1+M_{\rm w})^2\right) = -\epsilon. \tag{26}$$

Equation (26) can now directly be compared to Eq. (29) of Paper II, which represents the continuity equation of the wave energy flux in the absence of wind.

2.4. Limiting shock strength behavior

Similar to Paper II, we can now study the change of the residual shock strength $\hat{\alpha}$ (see Eq. (14)) with height. From Eqs. (17), (18), and (26) we obtain

$$\frac{1}{F_{\rm M}}\frac{{\rm d}F_{\rm M}}{{\rm d}r} = \frac{2}{\hat{\alpha}}\frac{{\rm d}\hat{\alpha}}{{\rm d}r} + \frac{3}{2}\frac{1}{H_{\rm T}} - \frac{1}{H_\rho} + \frac{a_{\rm w}}{H_{\rm w}} \tag{27}$$

with $H_{\rm T}$, H_ρ, and $H_{\rm w}$ as scale heights for the temperature, density, and the wind velocity, respectively, given by

$$H_{\rm T} = \left|\frac{1}{T_{\rm o}}\frac{{\rm d}T_{\rm o}}{{\rm d}r}\right|^{-1}, \tag{28}$$

$$H_\rho = \left|\frac{1}{\rho_{\rm o}}\frac{{\rm d}\rho_{\rm o}}{{\rm d}r}\right|^{-1}, \tag{29}$$

and

$$H_{\rm w} = \left|\frac{1}{M_{\rm w}}\frac{{\rm d}M_{\rm w}}{{\rm d}r}\right|^{-1}. \tag{30}$$

For the coefficient $a_{\rm w}$ we find

$$a_{\rm w} = \frac{2M_{\rm w}}{1+M_{\rm w}}. \tag{31}$$

As we want to apply our model preferably to longitudinal flux tube waves in solar and stellar chromospheres and winds, we assume in the following that the mean temperature $T_{\rm o}$ and Mach number of the wind $M_{\rm w}$ *increase* with height, whereas the mean density $\rho_{\rm o}$ *decreases* with height. Therefore, we must use $+H_{\rm T}^{-1}$, $-H_\rho^{-1}$, and $+H_{\rm w}^{-1}$ in Eq. (27). For other applications, the signs need to be adjusted accordingly.

Similar to Paper II, we also introduce the scale height of the geometrical dilution L given as

$$L = \left|\frac{1}{A}\frac{{\rm d}A}{{\rm d}r}\right|^{-1}, \tag{32}$$

which characterizes the spreading of the tube (or plume) as function of height. It should be noted that because of the conservation of the mass flux and magnetic flux, the various scale heights H_ρ, $H_{\rm T}$, $H_{\rm w}$, and L are not independent of each other. After some lengthy algebra, it can be shown that

$$\frac{1}{H_{\rm w}} = \frac{1}{H_\rho} - \frac{1}{2}\frac{1}{H_{\rm T}} - \frac{1}{L} + \frac{\beta}{2}\left(1+\frac{1}{2}\beta\gamma\right)^{-1} \times\left(\frac{1}{H_{\rm T}} - \frac{1}{H_\rho} + \frac{2}{L}\right). \tag{33}$$

Following Paper II, it is again possible to obtain solutions for the limiting residual shock strength $\hat{\alpha}_{\rm lim}$ attained at large heights. In case of ${\rm d}\hat{\alpha}/{\rm d}r \simeq 0$, we find

$$\hat{\alpha}_{\rm lim} \simeq \frac{c_{\rm So}P\mathcal{W}\mathcal{Z}}{4}\left(\frac{1}{H_\rho} - \frac{3}{2}\frac{1}{H_{\rm T}} - \frac{a_{\rm w}}{H_{\rm w}} - \frac{1}{L}\right) \tag{34}$$

with $\mathcal{W} = (1+M_{\rm w})^2$. Here we assume that the spreading of the tube (or plume) increases with height. Otherwise we have to use $+L^{-1}$ instead of $-L^{-1}$ as before. For $\mathcal{Z}(\beta)$ we obtain

$$\mathcal{Z}(\beta) = \frac{1+\frac{3}{2}\beta\gamma+\gamma}{(\gamma+1)(1+\frac{1}{2}\beta\gamma)^{\frac{1}{2}}}. \tag{35}$$

Equation (34) represents the expression for the limiting shock strength for longitudinal tube waves (or slow magnetosonic waves) in the presence of wind. By definition, $\hat{\alpha}$ cannot be negative (see Eq. (14)). Therefore, if a negative value (or a value relatively close to zero) is found by Eq. (34) because of H_ρ, $H_{\rm T}$, $H_{\rm w}$ and L, this equation is invalidated and $\hat{\alpha}_{\rm lim}$ must be computed following the more consistent approach outlined in Sect. 2.5. In this case, $\hat{\alpha}_{\rm lim}$ is given by Eq. (41).

Note that $\hat{\alpha}_{\rm lim}$ can either be larger or smaller than the limiting shock strength attained without wind depending on the values of $\mathcal{W}$ and $H_{\rm w}$. Clearly, if $\hat{\alpha}_{\rm lim}$ is too large, i.e., $\hat{\alpha}_{\rm lim} \gtrsim 0.3$, the results are highly inaccurate because the weak shock assumption is not met (see Paper I). The case without wind is given by $\mathcal{W} = 1$ and $a_{\rm w} = 0$, which allows us to identify Eq. (34) with Eq. (37) of Paper II. Note that Eq. (34) also includes the case of *acoustic waves* in stellar winds. In this case, we have to use $\mathcal{Z} = 1$ (see Paper II). For earlier results on the limiting shock strength behavior of acoustic waves see e.g. Ulmschneider (1970) and Cuntz & Ulmschneider (1988).

2.5. Derivation of $\hat{\alpha}(r)$

Equation (34) cannot be applied in cases where the limiting shock strength has not been attained or where $\hat{\alpha}_{\rm lim}$ is found to be negative. The first restriction is important in the region

$r \simeq r_o$, where the heating and energy dissipation are strongly affected by the amount of initial wave energy. In this case, we have to solve the differential equation for $\hat{\alpha}(r)$, which is a Riccati ODE (see Paper II, Appendix B). With $z = r - r_o$ we find

$$W = \frac{1}{H_\rho} - \frac{3}{2}\frac{1}{H_T} - \frac{a_w}{H_w} - \frac{1}{L} \tag{36}$$

and

$$K = \frac{4}{c_{So} P \mathcal{W} \mathcal{Z}}. \tag{37}$$

Here H_T, H_ρ, H_w and L are permitted to be dependent on radius r, which is formally incompatible with the derivation of Eq. (34).

With the substitutions

$$W^* = \frac{1}{z}\int_0^z W(z')\mathrm{d}z' \tag{38}$$

and

$$I = \frac{1}{2} W^* \, \mathrm{e}^{-\frac{1}{2}W^* z} \int_{-\infty}^{z} \mathrm{e}^{\frac{1}{2}W^* z'} \mathrm{d}z' \tag{39}$$

we obtain as general solution for $\hat{\alpha}(r)$

$$\hat{\alpha} = \left(\frac{KI}{W^*} + \left(\frac{1}{\hat{\alpha}_o} - \frac{KI}{W^*} \right) \mathrm{e}^{-\frac{1}{2}W^* z} \right)^{-1} \tag{40}$$

(see Paper II). Here we determined the integration constant by taking $\hat{\alpha} = \hat{\alpha}_o$ for $r = r_o$ as inner boundary condition. For large values of r, we obtain

$$\hat{\alpha}_{lim} = \frac{W^*}{KI}. \tag{41}$$

In case that W^* is essentially independent of r, we find $W^* \simeq W$ and $I \simeq 1$ implying

$$\hat{\alpha}_{lim} \simeq \frac{W}{K} \tag{42}$$

in agreement with Eq. (34).

2.6. The modified energy dissipation law

Next we want to derive the energy dissipation law for longitudinal tube waves considering the influence of a stellar wind. Here we consider the generalized case of waves not necessarily obeying limiting shock strength behavior. By introducing $\epsilon^* = \epsilon / F_M$, given by

$$\epsilon^* = \frac{4(\gamma+1)}{(1 + \frac{3}{2}\beta\gamma + \gamma)\lambda} \hat{\alpha}, \tag{43}$$

with $\lambda = c_{To} P$ as wavelength, we find using Eq. (26)

$$\frac{1}{F_M}\frac{\mathrm{d}F_M}{\mathrm{d}r} + \frac{1}{A}\frac{\mathrm{d}A}{\mathrm{d}r} + \frac{2}{1+M_w}\frac{\mathrm{d}M_w}{\mathrm{d}r} = -\epsilon^{**} \tag{44}$$

with $\epsilon^{**} = \epsilon^*/(1+M_w)^2$. The scale height of the wave energy flux is given by

$$H_F = \left| \frac{1}{F_M}\frac{F_M}{\mathrm{d}r} \right|^{-1}. \tag{45}$$

Hence, with Eqs. (30), (32), (44), and (45), the scale height for the decrease of the wave energy flux with height can be expressed by

$$H_F = \left(\frac{\epsilon^*}{(1+M_w)^2} + \frac{2M_w}{1+M_w}\frac{1}{H_w} + \frac{1}{L} \right)^{-1}. \tag{46}$$

Equation (46) is particularly useful for evaluating the change of wave heating rates with height in models of different spreading functions and wind velocities (see Sect. 3.2). With H_F^{stat} as scale height of the wave energy flux in the absence of wind (see Eq. (39); Paper II), we find

$$\frac{1}{H_F} = \frac{1}{H_F^{stat}} + \frac{2M_w}{1+M_w}\frac{1}{H_w} - \frac{M_w(2+M_w)}{(1+M_w)^2}\epsilon^*. \tag{47}$$

Equation (47) shows that the scale height for the decrease of the wave energy flux for waves with significant dissipation is always larger in models with wind being present. This means that due to the wind, the wave energy dissipates more slowly with height, as expected.

3. Applications to wave models of solar plumes

3.1. Model assumptions

A study case of longitudinal waves (also called slow magnetosonic waves) propagating in stellar winds is the case of solar plumes. Plumes are ray-like density enhancements in solar coronal holes. Understanding the dynamics of solar plumes may be crucial for unravelling the mass and energy balance of the solar corona and wind. DeForest & Gurman (1998) identified slow magnetosonic waves with a wave energy flux F_M between 1.5×10^5 and 4.0×10^5 erg cm^{-2} s^{-1} with wave periods ranging from 10 to 15 min. The wave amplitudes implied by the observations are between 7.5 and 15.0 km s^{-1}. Ofman et al. (1999) estimated that slow magnetosonic waves can provide between 0.02 and 0.30 of the total energy required to heat and accelerate the fast solar wind.

A subsequent study of Cuntz & Suess (2001) showed that shock formation in coronal plumes occurs at rather low heights, i.e., between 1.1 and 1.3 $R_\odot$, depending on the wave parameters. This implies that shock heating via slow magnetosonic waves is expected to be relevant at most heights. In addition, it is found that due to the very low values of plasma-β in solar plumes (i.e., between 2×10^{-4} and 1×10^{-6}), the slow magnetosonic waves are very close to the case of acoustic waves. Here we want to study the effects of energy dissipation by slow magnetosonic waves based on our analytical concept. The plume parameters are identical to those used by Cuntz & Suess. Our models assume a single-fluid medium with a temperature of $T = 10^6$ K. The initial density model assumes a hydrogen number density of 1.2×10^8 cm^{-3} at the inner radius $r_o = 1.01\ R_\odot$. At r_o, we also assume a magnetic field strength of 100 G and a plume opening radius of 1000 km. The assumed density model given by $\rho \sim r^{-8.785}$ closely follows the height distribution of the electron density in White-Light polar plumes (Koutchmy & Bocchialini 1998; see also results by Giordano et al. 2000), which allows one to constrain the flow speed of the wind $u_o(r)$. We adopt the same area function $A(r)$ already used by

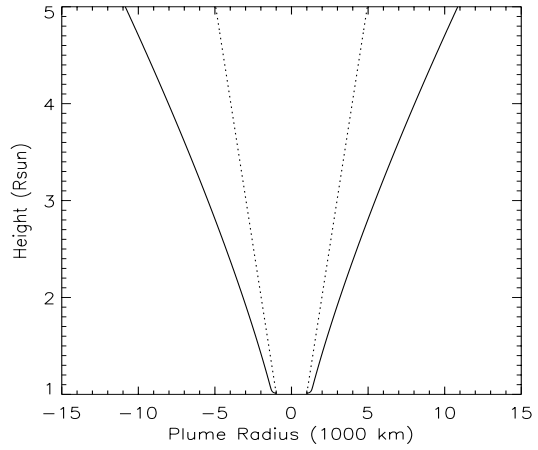

Fig. 1. Plume geometry between 1.01 and 5 $R_\odot$ (solid lines) with spherical geometry given for comparison (dotted lines).

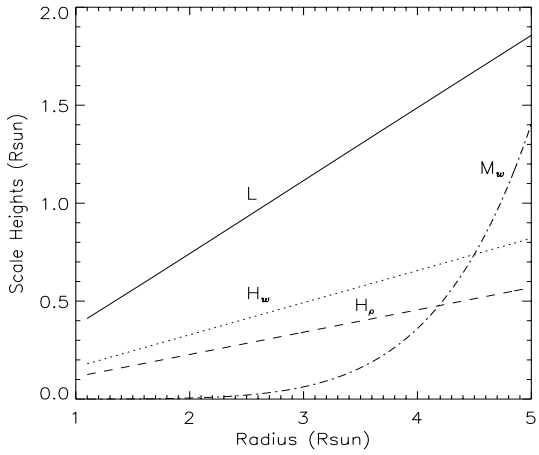

Fig. 2. Scale height of the geometrical dilution L (solid line), density H_ρ (dashed line), and velocity of the stellar wind H_w (dotted line) as function of radius. For comparison, we also give the Mach number $M_\mathrm{w} = u_\mathrm{o}/c_\mathrm{To}$ (dash-dotted line).

Cuntz & Suess (see Fig. 1), which was deduced following Suess (1998) and Suess et al. (1998) based on empirical constraints mostly from SOHO/UVCS (see Appendix B). Earlier theoretical predictions for the area functions of coronal plumes and coronal holes have been given by Kopp & Holzer (1976), Habbal et al. (1995), and Hu et al. (1997).

3.2. Results

The analytical methods derived in Sect. 2 allow one to study the effects of the solar wind on the propagation of slow magnetosonic waves (i.e., longitudinal tube waves) in coronal plumes. In particular, we are able to assess the influence of the spreading of the plume and of the wind velocity profile on the strength of the shock wave. The strength of the shock wave $M_\mathrm{s} = 1 + \hat{\alpha}$ is directly related to the amplitudes of the temperature, pressure, density, magnetic field strength, and other quantities as well (see Appendix B). Here we focus on the behavior of the limiting shock strength $\hat{\alpha}_\mathrm{lim}$ (see Eqs. (34), (42)) as function of height. The limiting shock strength critically depends on the various scale heights of the atmosphere, i.e., H_ρ, H_T, H_w,

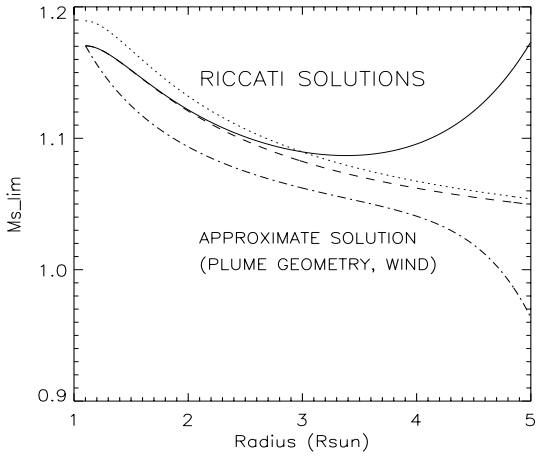

Fig. 3. Behavior of the limiting shock strength $M_\mathrm{s}^\mathrm{lim} = 1 + \hat{\alpha}_\mathrm{lim}$ for different cases, which are: plume geometry with wind (solid line), plume geometry without wind (dashed line), and spherical geometry without wind (dotted line). These models are based on solutions of the Riccati ODE (see Eq. (41)). For the case of plume geometry with wind, we also give the approximate solution based on Eq. (34), Sect. 2.4 (dash-dotted line). The depicted models assume a wave period of 10 min.

and L (see Fig. 2). Clearly, since the atmosphere is assumed as isothermal, we have $H_\mathrm{T}^{-1} = 0$.

Figure 3 depicts the behavior of the limiting shock strength with plume geometry and wind in comparison with the case without wind. It is found that the limiting shock strength decreases at the inner part of the atmosphere, and then increases beyond 3.5 $R_\odot$. This is a consequence of the $\mathcal{W} = (1 + M_\mathrm{w})^2$ term and the increase of the Mach number M_w as function of height. Assuming a wave period of 10 min, the limiting shock strength $M_\mathrm{s}^\mathrm{lim}$ with plume geometry and wind at 5 $R_\odot$ is equal to 1.17, whereas in the model without wind, the shock strength is equal to 1.05. Note, however, that these models should not be extended to larger heights because this would result in increasing larger values of M_s, which would invalidate the assumption of weak shocks (see Paper I). These calculations for the limiting shock strength are based on consistent solutions of the Riccati ODE (see Sect. 2.5) considering that the approximate solution (see Sect. 2.4) would result in unrealistic (negative) values for $\hat{\alpha}$ due to the behavior of the various scale heights. We also inspected the limiting shock strength for the case of spherical geometry without wind. We found that in this case, consistently higher values of $M_\mathrm{s}^\mathrm{lim}$ are attained compared to the case of plume geometry due to the lesser dilution of the wave energy flux as function of height.

A further topic of interest is the study of the influence of the solar wind on the damping length of the wave energy flux. Figure 4 shows a variety of theoretical models, which differ regarding the selected wave amplitude, wave period and inclusion of the wind. As amplitudes, we have taken 7.5 and 15.0 km s^{-1} (Ofman et al. 1999), corresponding to shock strength of $M_\mathrm{s} = 1.07$ and 1.14, respectively, which efficiently ensures that the weak shock approximation is applicable. In the models calculated, it is found that the wave energy damping

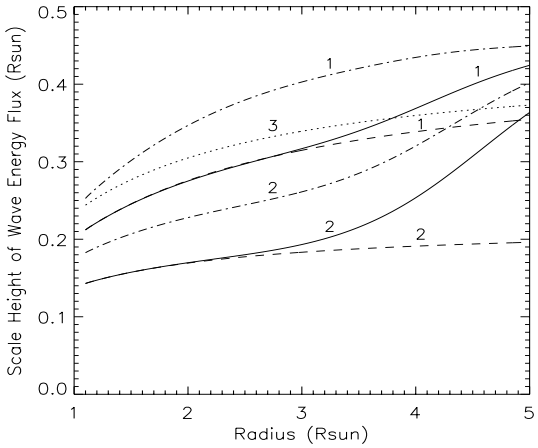

Fig. 4. Wave energy damping length for a variety of models. We show two sets of curves consisting of three lines each, belonging to the following models: plume geometry without wind, P = 10 min (dashed lines) and plume geometry with wind, P = 10 min (solid lines) and P = 15 min (dashed-dotted lines). For the upper set of curves (1), the wave amplitudes are 7.5 km s^{-1}, whereas for the lower set of curves (2) they are 15 km s^{-1} instead. For comparison, we also show the case of spherical symmetry, no wind, for waves of P = 10 min and 7.5 km s^{-1} (dotted line), see curve (3).

length ranges between 0.15 $R_\odot$ and 0.45 $R_\odot$, and furthermore increases as function of height.

For wave models with periods of 10 min, we studied the role of the solar wind in the spatial increase of the wave energy damping length in particular detail. We found that the cases with wind and without wind were virtually identical below 2.3 $R_\odot$ for M_s = 1.14 and below 3.1 $R_\odot$ for M_s = 1.07. However, at larger heights, the wave energy damping lengths in models with wind were found to be larger. At radius 5 $R_\odot$, the increase of the wave energy damping length in the M_s = 1.07 model was found to be 20%, whereas in the M_s = 1.14 model, it was found to be as large as 85%. This shows that the "carry-along effect" of the wind, i.e., its ability to reduce the spatial decrease of the wave energy flux with height, is of pivotal importance for the energy dissipation of the waves. In this respect, the carry-along effect may even surpass the relevance of the plume geometry as shown through test calculations with the plume geometry replaced by spherical geometry. We also calculated models with wave periods of 15 min. It was found that the wave energy damping length is usually larger than in models with 10 min period waves, as expected.

4. Conclusions

We investigated the analytic properties of longitudinal tube waves in case of small amplitudes taking into account ambient wind flows. We found that through the inclusion of the wind, the dynamical properties of the waves are significantly altered, including their limiting shock strength behavior. Stellar winds can either increase or decrease the limiting shock strength of the waves, depending on the wind parameters.

The limiting shock strength is best be represented by a consistent solution of the Riccati ODE, which is more accurate than the approximate solution. The reason is that the limiting residual shock strength $\hat{\alpha}_{\rm lim}$ given by the approximate solution can be close to zero (but still positive) or negative, resulting in unreliable or unphysical values for $\hat{\alpha}_{\rm lim}$, respectively. This behavior is due to the values of $H_{\rm T}$, H_ρ, $H_{\rm w}$, and L, i.e., the scale heights for the temperature, density, wind velocity, and geometrical dilution, respectively. In case that the residual shock strength is larger than about 0.3, no reliable estimates can be given based on the analytic assessment of the waves (see also Paper I). In principle, the weak shock approximation is expected to underestimate the shock heating rates as pointed out by Cuntz & Ulmschneider (1988) for static atmospheres, even though detailed models would be required to attain detailed comparisons for dynamic atmospheres. Our results are also directly applicable to acoustic waves in stellar winds since longitudinal waves are identified as acoustic waves in case of plasma-β = 0.

As an application, we studied the properties of longitudinal waves (also referred to as slow magnetosonic waves) in solar plumes. Following Cuntz & Suess (2001), slow magnetosonic waves form shocks at rather low coronal heights, i.e., between 1.1 and 1.3 $R_\odot$, depending on the model parameters. Taking wave amplitudes and wave periods given by observations, we studied the effects of solar wind flows on the damping length of the wave energy flux. We found that the damping length of the wave energy flux increases up to 85% through the "carry-along effect" by the wind. This effect was found to be largest for high-amplitude waves. The carry-along effect of the wind efficiently offsets the dilution of the wave energy by the plume geometry given by the increase of the plume spreading with height. These findings are a strong motivation for further studies of wave propagation in solar-type winds to be based on self-consistent time-dependent simulations.

Acknowledgements. This work has been supported by the UAH/USRA/NASA Cooperative Agreement on Research in Space Plasma Physics (M.C.), by NSF under grant ATM-0087184 (M.C.) and the Ulysses/SWOOPS experiment team (S.T.S.).

Appendix A: Shock amplitude relations

Here we summarize the normalized shock amplitudes $u'_{\rm m}$, $\rho'_{\rm m}$, $p'_{\rm m}$, $T'_{\rm m}$, $B'_{\rm m}$, $A'_{\rm m}$, $c'_{\rm Sm}$, $c'_{\rm Am}$ and $c'_{\rm Tm}$ given as e.g. $\rho'_{\rm m} = \rho_{\rm m}/\rho_{\rm o}$ with $\rho_{\rm m} = (\rho_2 - \rho_1)/2$ and $\rho_{\rm o} = (\rho_1 + \rho_2)/2$ and so on[1]:

$$u'_{\rm m} = \frac{2}{\gamma + 1}\,\xi\hat{\alpha} \tag{A.1}$$

$$\rho'_{\rm m} = \frac{2}{\gamma + 1}\left(1 + \frac{1}{2}\beta\gamma\right)^{-1}\,\xi\hat{\alpha} \tag{A.2}$$

$$p'_{\rm m} = \frac{2\gamma}{\gamma + 1}\left(1 + \frac{1}{2}\beta\gamma\right)^{-1}\,\xi\hat{\alpha} \tag{A.3}$$

$$T'_{\rm m} = \frac{2(\gamma - 1)}{\gamma + 1}\left(1 + \frac{1}{2}\beta\gamma\right)^{-1}\,\xi\hat{\alpha} \tag{A.4}$$

[1] Note the difference in the definition of $u'_{\rm m}$ in comparison with the other variables (see Paper I, p. 1103).

$$B'_{\rm m} = \frac{2}{\gamma+1}\left(1-\left(1+\frac{1}{2}\beta\gamma\right)^{-1}\right)\xi\hat{\alpha} \tag{A.5}$$

$$A'_{\rm m} = \frac{2}{\gamma+1}\left(1-\left(1+\frac{1}{2}\beta\gamma\right)^{-1}\right)\xi\hat{\alpha} \tag{A.6}$$

$$c'_{\rm Sm} = \frac{\gamma-1}{\gamma+1}\left(1+\frac{1}{2}\beta\gamma\right)^{-1}\xi\hat{\alpha} \tag{A.7}$$

$$c'_{\rm Am} = \frac{1}{\gamma+1}\left(2-\left(1+\frac{1}{2}\beta\gamma\right)^{-1}\right)\xi\hat{\alpha} \tag{A.8}$$

$$\begin{aligned} c'_{\rm Tm} = & \left(\frac{\gamma-1}{\gamma+1}\left(1+\frac{1}{2}\beta\gamma\right)^{-2}-\frac{1}{\gamma+1}\left(1-\left(1+\frac{1}{2}\beta\gamma\right)^{-1}\right)\right. \\ & \left.\times\left(2-\left(1+\frac{1}{2}\beta\gamma\right)^{-1}\right)\right)\xi\hat{\alpha} \end{aligned} \tag{A.9}$$

with ξ given by

$$\xi = \frac{(\gamma+1)\left(1+\frac{1}{2}\beta\gamma\right)^2}{1+\frac{3}{2}\beta\gamma+\gamma}. \tag{A.10}$$

Here u is the flow speed, ρ the density, p the gas pressure, T the temperature, B the magnetic field strength, A the tube cross section, $c_{\rm S}$ the adiabatic sound speed, $c_{\rm A}$ the Alfvén speed, and $c_{\rm T}$ the tube speed. Note that the shock amplitude relations only depend on $\hat{\alpha}$, i.e. the residual shock strength (see Eq. (14)), and plasma-β.

Appendix B: Area function of solar plumes

The area function $A(r)$ used for the computation of solar plume models can be parameterized as

$$A(r) = A_{\rm o}\left(\frac{r}{r_{\rm o}}\right)^2 f(r) \tag{B.1}$$

where $A_{\rm o}f(r_{\rm o})$ is the area of the plume at its base, i.e. at radius $r_{\rm o}$, and $f(r)$ is the spreading factor. Suess (1998) and Suess et al. (1998) assumed that the spreading factor can be considered as existing of two parts, i.e. the local spreading $f_{\rm l}(r)$ and the global spreading $f_{\rm g}(r)$ with $f(r)$ given by

$$f(r) = f_{\rm l}(r)f_{\rm g}(r). \tag{B.2}$$

Following Suess et al. (1998), it is found that

$$f_{\rm l}(r) = 1 + 13.31\cdot\left(1-{\rm e}^{-\frac{r/R_\odot-1}{0.011}}\right) \tag{B.3}$$

and

$$f_{\rm g}(r) = a_0 + a_1\frac{r}{R_\odot} + a_2\left(\frac{r}{R_\odot}\right)^2 + a_3\left(\frac{r}{R_\odot}\right)^3 + a_4\left(\frac{r}{R_\odot}\right)^4 \tag{B.4}$$

with $R_\odot$ as solar radius, and $a_0 = 0.24974$, $a_1 = 0.76714$, $a_2 = -0.085164$, $a_3 = 0.0093196$, and $a_4 = -0.0004403$. These numbers are for a typical plume base field strength of 20 times the interplume field and a large coronal hole. The local spreading $f_{\rm l}(r)$ is important below 35 000 km, varies rapidly at these heights, and is constant above that height. The global spreading $f_{\rm g}(r)$ varies much more slowly at those heights. The behavior of $f_{\rm g}(r)$ is largely given by the coronal hole geometry. We find $f_{\rm l} \simeq 14$ at 1.2 $R_\odot$ and $f_{\rm g} \simeq 2.8$ and $f \simeq 41$ at 5 $R_\odot$.

References

Bretherton, F. P. 1970, in Mathematical Problems in the Geophysical Sciences, Providence, American Mathematical Society, 61

Casalbuoni, S., Del Zanna, L., Habbal, S. R., & Velli, M. 1999, J. Geophys. Res., 104, 9947

Cuntz, M. 1999, A&A, 350, 1100 (Paper I)

Cuntz, M. 2004, A&A, 420, 699 (Paper II)

Cuntz, M., & Suess, S. T. 2001, ApJ, 549, L143

Cuntz, M., & Ulmschneider, P. 1988, A&A, 193, 119

Cuntz, M., Ulmschneider, P., & Musielak, Z. E. 1998, ApJ, 493, L117

Cuntz, M., Rammacher, W., Ulmschneider, P., Musielak, Z. E., & Saar, S. H. 1999, ApJ, 522, 1053

DeForest, C. E., & Gurman, J. B. 1998, ApJ, 501, L217

Del Zanna, L., Hood, A. W., & Longbottom, A. W. 1997, A&A, 318, 963

Fawzy, D. E., Ulmschneider, P., & Cuntz, M. 1998, A&A, 336, 1029

Gabriel, A. H., Bely-Dubau, F., & Lemaire, P. 2003, ApJ, 589, 623

Giordano, S., Antonnucci, E., Noci, G., Romoli, M., & Kohl, J. L. 2000, ApJ, 531, L79

Habbal, S. R., Esser, R., Guhathakurta, M., & Fisher, R. R. 1995, Geophys. Res. Lett., 22, 1465

Herbold, G., Ulmschneider, P., Spruit, H. C., & Rosner, R. 1985, A&A, 145, 157

Holzer, T. E., & MacGregor, K. B. 1985, in Mass Loss from Red Giants, ed. M. Morris, & B. Zuckerman (Dordrecht: Reidel), 229

Hu, Y.-Q., Esser, R., & Habbal, S. R. 1997, J. Geophys. Res., 102, 661

Jacques, S. A. 1977, ApJ, 215, 942

Jordan, C., & Linsky, J. L. 1987, in Exploring the Universe with the IUE Satellite, ed. Y. Kondo et al. (Dordrecht: Kluwer), 259

Kopp, R. A., & Holzer, T. E. 1976, Sol. Phys., 49, 43

Koutchmy, S., & Bocchialini, K. 1998, in Solar Jets and Coronal Plumes, ESA SP-421, 51

Landau, L. D., & Lifshitz, E. M. 1987, Fluid Mechanics, Course of Theoretical Physics, 2nd Ed. (Oxford: Pergamon Press)

Linsky, J. L. 1980, ARA&A, 18, 439

Narain, U., & Ulmschneider, P. 1990, Space Sci. Rev., 54, 377

Narain, U., & Ulmschneider, P. 1996, Space Sci. Rev., 75, 453

Ofman, L., Romoli, M., Poletto, G., Noci, G., & Kohl, J. L. 1997, ApJ, 491, L111

Ofman, L., Romoli, M., Poletto, G., Noci, G., & Kohl, J. L. 1998, ApJ, 507, L189

Ofman, L., Nakariakov, V. M., & DeForest, C. E. 1999, ApJ, 514, 441

Ofman, L., Nakariakov, V. M., & Sehgal, N. 2000, ApJ, 533, 1071

Pijpers, F. P., & Hearn, A. G. 1989, A&A, 209, 198

Rammacher, W., & Ulmschneider, P. 1989, in Solar and Stellar Granulation, ed. R. J. Rutten, & G. Severino (Dordrecht: Kluwer), 589

Roberts, B. 1983, Sol. Phys., 87, 77

Schrijver, C. J., & Title, A. M. 2003, ApJ, 597, L165

Schüssler, M., Caligari, P., Ferriz-Mas, A., & Moreno-Insertis, F. 1994, A&A, 281, L69

Solanki, S. K. 1996, in Stellar Surface Structure, ed. K. G. Strassmeier, & J. L. Linsky (Dordrecht: Kluwer), IAU Symp., 176, 201

Spruit, H. C. 1981, A&A, 98, 155

Spruit, H. C. 1982, Sol. Phys., 75, 3

Suess, S. T. 1998, in Solar Jets and Coronal Plumes, ESA SP-421, 223

Suess, S. T., Poletto, G., Wang, A.-H., Wu, S. T., & Cuseri, I. 1998, Sol. Phys., 180, 231

Ulmschneider, P. 1970, Sol. Phys., 12, 403

Wood, B. E., Müller, H.-R., Zank, G. P., & Linsky, J. L. 2002, ApJ, 574, 412